www.czasopisma.pan.pl PAN www.journals.pan.pl

jet INTL JOURNAL OF ELECTRONICS AND TELECOMMUNICATIONS, 2023, VOL. 69, NO. 3, PP. 439-448
Manuscript received February 9, 2023; revised July, 2023. DOI: 10.24425/ijet.2023.144381

A New Diminutive Wide-band MIMO Antenna with Frequency Agile Features for 4G and 5G Diverse Wireless Applications

Shivleela Mudda, Gayathri K M, and Mallikarjun M

***Abstract*—This paper demonstrates a low-profile, wide-band, two-element, frequency-reconfigurable MIMO antenna that is suitable for diverse wireless applications of 4G and 5G such as WLAN/Bluetooth (2.4–2.5 GHz), WLAN (2.4–2.484 GHz, 5.15–5.35 GHz, and 5.725–5.825 GHz), WiMAX (3.3–3.69 GHz and 5.25–5.85 GHz), Sub6GHz band proposed for 5G (3.4–3.6 GHz, 3.6-3.8GHz and 4.4–4.99 GHz), INSAT and satellite X-band(6 to 9.6 GHz). Proposed MIMO favour effortless switching between multiple bands ranging from 2.2 to 9.4 GHz without causing any interference. Both antenna elements in a MIMO array are made up of a single module comprised of a slot-loaded patch and a defective structured ground. Two PIN diodes are placed in the pre-set position of the ground defect to achieve frequency-reconfigurable qualities. The suggested MIMO antenna has a size of 62 ×25 ×1.5 mm^3. Previous reconfigurable MIMO designs improved isolation using a meander line resonator, faulty ground structures, or self-isolation approaches. To attain the isolation requirements of modern devices, stub approach is introduced in proposed design. Without use of stub, simulated isolation is 15dB. The addition of a stub improved isolation even more. At six resonances, measured isolation is greater than 18 dB, the computed correlation coefficient is below 0.0065, and diversity gain is over 9.8 dB.**

***Keywords*—Diversity gain (DG); Defective ground structure (DGS); Fractional bandwidth (FBW); ITU (International telecommunication union); INSAT; Frequency Reconfigurable antenna (FRA); Multiple input multiple output (MIMO); Mutual coupling; Isolation; 5G; Envelope correlation coefficient (ECC)**

I. INTRODUCTION

FIFTH-generation (5G) wireless communication has received a lot of interest in recent years. The rapid increase in portable device traffic is the driving force behind the intense interest in the development of 5G technology. With the exponential growth of wireless devices, a variety of issues have emerged, such as spectrum congestion, lower data rates, reduced channel capacity, improper spectrum usage, interference, and jamming. 4G technological innovations were inefficient to quench the modern era's need. Wider operating bandwidth is helpful in enhancing channel capacity and data rates in current and future generation devices [1]. An antenna is an element mean for radiation and reception of signals that reveal information. Industry sponsors' requirements for 5G antenna design include frequency tuning, low cost, wide bandwidth, a steady radiation pattern, increased channel capacity, and improved link reliability. Such requirements cannot be met by a single antenna. To satisfy the aforesaid needs, 5G employs MIMO antennas [2]. The FCC has designated a sub-6 GHz (3.2 to 6 GHz) frequency band for 5G wireless communication since it can provide improved spectral efficiency in the available spectrum and facilitate network development in urban areas [3]. As portable devices are becoming lighter and thinner by the day, a typical MIMO antenna for 5G devices should meet specified criteria like compact structure with high gain, steady radiation pattern, and low envelop correlation [4]. The most effective way to make MIMO compact is to replace multiple fixed-performance antennas of MIMO with frequency-reconfigurable antennas, which provide coverage for several wireless applications on the same platform based on switching conditions [5]. FRA also aids in maintaining high data rate and adequate isolation between antenna units within MIMO [6].

MIMO's close proximity of radiating units provides compactness at the expense of high mutual coupling, which reduces throughput. A compact MIMO antenna design with good performance and the additional need for tunable behavior is a significant issue for portable devices. Various external and internal decoupling strategies have been reported to construct a MIMO antenna system with excellent element isolation [7]. These methods can modify coupling by constricting, blocking, or reducing surface current flow.

Several MIMO frequency reconfigurable antennas for 4G, 5G, S-band, and X-band applications are documented in the literature. However, the majority of them focused on single-band MIMO, a few on multiband, and a very few on FR-MIMO antennas. A triband, dual-port FRA MIMO system based on C-structured defects in the patch and four-pin diodes was proposed in a paper [8]. The designed MIMO antenna has an overall volume of 60 ×20 ×0.8 mm^3. This achieves good isolation by incorporating an inverted T-shaped defect between the elements. To improve isolation, a unique C-structured meandered-line-resonator (MLR) is placed on top between elements. A frequency reconfigurable quad-band MIMO antenna designed on the basis of complex structure of a ring and new moon is presented in [9]. To diminish mutual coupling between close elements, a gradient arc structure is utilized, which is challenging to achieve. The antenna is 71 x 30 x 1.6 mm^3 in overall volume. Due to the near proximity of the

Shivleela Mudda and Gayathri K M are with Dayananda Sagar University, Bangalore, India (e-mail: muddass1982@gmail.com, gayathri-ece@dsu.edu.in).

Mallikarjun M is with Srinidhi Institute of Science and Technology, Hyderabad (Telangana), India (e-mail: mudda77@gmail.com).

elements, the S21 values are typically less than -15dB. A meandering slot-line-based quad-band MIMO system with sub-1 GHz spectrum coverage and multiband functioning is delineated in [10]. MIMO is realized on a RO4350 substrate with 60 ×120× 0.76 mm^3 dimensions. The antenna covers the frequencies 0.665–1.13 GHz, 1.415–2.005 GHz, 2.42–3.09 GHz, and 3.18–3.89 GHz. Over the all-operating bands, the worst-case isolation values found were -11.7dB. A MIMO antenna for 4G and early 5G wireless communication is described in a paper [11]. The actual size of this antenna is 120 mm× 60 mm ×1.52 mm^3. Two antennas are placed orthogonally to each other on the same substrate to improve diversity performance. The observed S12 between the elements is also good, measuring 16 dB for resonance mode-1 and 19 dB for resonance mode-2.In [12], MIMO seems to have a volume of 32× 98× 1 mm^3, where measured S12 is greater than 15 dB. The antenna switches between 1.8, 2.4, 3.5, and 5.5 GHz bands with ECC< 0.04. In [13], I-shaped stubs are loaded to attain good S12 in a semi-circular contour MIMO antenna functioning over a frequency range of 1.9 to 10.2 GHz, whereas the reported antenna is 27×50 mm^2 in size, which is larger and non-reconfigurable in comparison.

The designs discussed above achieve a compromise between massive size, narrow bandwidth, and design complexity. The positioning of the meander line resonator in [8] is difficult and makes the fabrication complex. The designs given in [9,10,11] have the disadvantage of being larger and hence more difficult to apply to portable devices. According to [12], widespread use of MEMS causes significant insertion loss. Similarly, in [9, 10] the antenna isolation is insufficient to meet the modern MIMO norm of more than 15dB. There were only a few stub-based antennas in the literature, and they were all non-reconfigurable with restricted frequency band coverage. Furthermore, the literature focuses mostly on frequency reconfigurable MIMO antennas for 4G or sub-6 GHz bands. As a result, wide band frequency-reconfigurable MIMO antennas covering 4G/LTE, all Sub 6GHz bands with higher frequency bands are an appealing field of research for current and next-generation wireless applications.

In this article, a new easy-to-integrate, small, two-element, frequency-reconfigurable MIMO antenna operating over 2.2 to 9.4 GHz with a wide-bandwidth ranging from 900MHz to 6800MHz is investigated for modern generation wireless device applications. Based on the switching conditions, the suggested antenna covers six communicating frequency bands: f1 = 8.9, f2 = 3.5, f3 = 8.7 GHz, f4 = 3.4, f5=8.4, and f6 = 5.4 GHz. The presented MIMO provides an adequate level of isolation of -15dB without stub loading. The integration of a stub improved isolation even more. Isolation greater than 18dB is measured at different operating frequencies. The calculated coupling coefficient and CCL is less than 0.0065 and 0.2bps/Hz. Also, diversity gain of almost 10 dB is achieved in these working bands.

II. SINGLE ELEMENT ANTENNA

This section presents the design and analysis of a DGS-based FRA that operates in four modes. PIN diodes that differentially control the flow of current in the antenna structure are used to shift or switch modes. The single antenna operates between six communicating frequency bands centred at f1 = 8.9, f2 = 2.9, f3 = 8.7 GHz, f4 = 3, f5=8.6, and f6 = 5.6 GHz based on switching states. FRA is implemented on a 1.5-mm-thick FR-4 substrate with a dielectric permittivity of 4.2 and a loss tangent of 0.02. A single antenna element is 25× 28 mm^2 in size. This antenna is powered by a 50-ohm microstrip feed line in typical operation.

The proposed single element has wide-band characteristics. Figures 1(a) and (b) illustrates the proposed single element's evolution steps and corresponding reflection coefficients. First, a complete ground-plane microstrip-line-fed rectangular patch antenna with a resonance frequency of 6.8 GHz is modeled. The observed reflection coefficient at this frequency is -11 dB. Step 2 entails etching slots into the rectangular patch and shrinking the ground dimensions to 6.5×25mm^2. To reconfigure the surface conductance, a fragmented ground plane was inserted beneath the feed line. The use of a partial ground plane changed the characteristic impedance and, as a result, the S-parameters. The impedance bandwidth observed is less than -10 dB at operating frequencies of 3.4 and 7.8 GHz. Steps 3 and 4 engrave nearly one F-shaped DGS (slot1) with a 20× 1mm^2 size and one nearly U-shaped DGS (slot2) with a length of less than λ/4, resulting in matching bandwidth at the 3.2–8.6 GHz and 2.2–9.4 GHz bands.

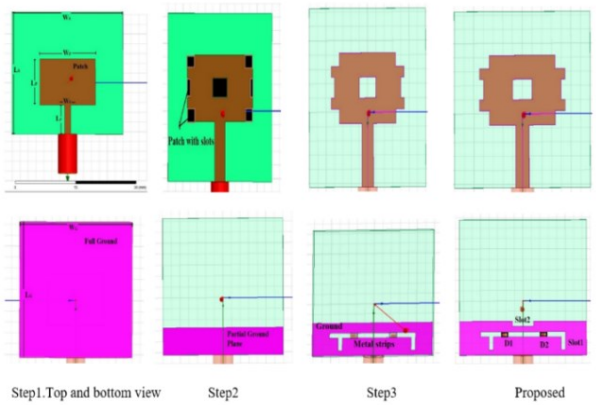

(a)

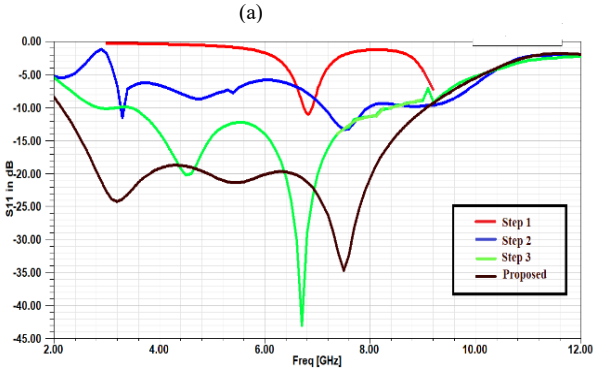

(b)

Fig. 1. (a) Design steps (b) Evolution steps reflection coefficient

The proposed FRA antenna is implemented in stage4 by incorporating two SMP-1320-SC79 PIN diodes (D1 and D2). In the ANSYS high-frequency structure simulator, the FRA

antenna is simulated using diodes with 0.9 ohms resistance to turn on and a 0.3 pF capacitor to turn off. For dc biasing of D1 and D2, 0.6mm× 2mm copper strips are formed within the F-DGS at the diode placement position. In addition, a 100-pF DC blocking capacitor is linked in series with the diodes (refer to Figure 2). A voltage of 1 volt and 5volts is enough to switch the PIN diode between the ON and OFF states.

Figure 3 depicts the measured S11 of fabricated FRA in various modes. Impedance bandwidth reference of -10 dB is achieved at 8.4–9.5 GHz (FBW = 21.53%) in mode-1(when diodes OFF) with S11 of -13.74 at 8.9 GHz. Dual-band operation has been measured in switching state 2 (D1, D2 ON/OFF) at 2.4–3.5 GHz (18.38%) and 6.2–9.6 GHz (56.03%) bands, with an observed S11 of -12.58 dB and -26 dB, respectively. In switching state 3 (OFF/ON), evaluated findings demonstrate impedance bandwidths of -10 dB at 2.4–3.7 GHz (18.38%) and 6–9.6 GHz (57%) at 3 GHz and 8.6 GHz bands, respectively. Operation is observed over the 2.4–9.2 GHz (103.07%) band for state 4 (both ON), with an S11 of -22.36 at the 5.6 GHz center frequency.

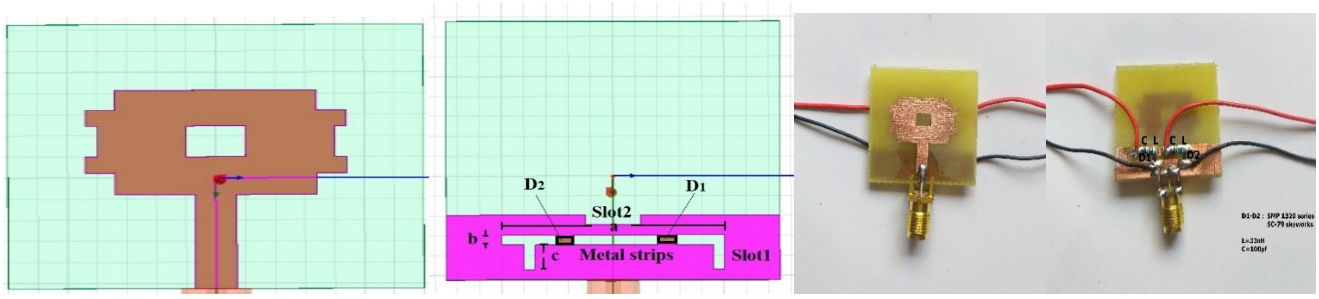

Fig. 2. Schematics and fabricated top and bottom views of proposed single element

TABLE I
STRUCTURAL PARAMETERS OF A SINGLE-ELEMENT ANTENNA

Parameters	*Value(mm)*	*Parameters*	*Value(mm)*
Length of the patch (L_P)	9.8	Length of feed (L_F)	6
Width of the patch (W_P)	13	Width of feed (W_F)	2.8
Substrate and full ground length (L_S=L_G)	25	Ground plane slot1 (a×b×c)	20×1×1.4mm^2
Substrate and ground width (W_S=W_G)	28	Metal strips	0.6mm × 2 mm
Patrial Ground length (L_{PG})	6.5	Ground plane slot2 (d×e)	1.8mm×1mm
Ground width (W_G)	28	Height of substrate (h)	1.5

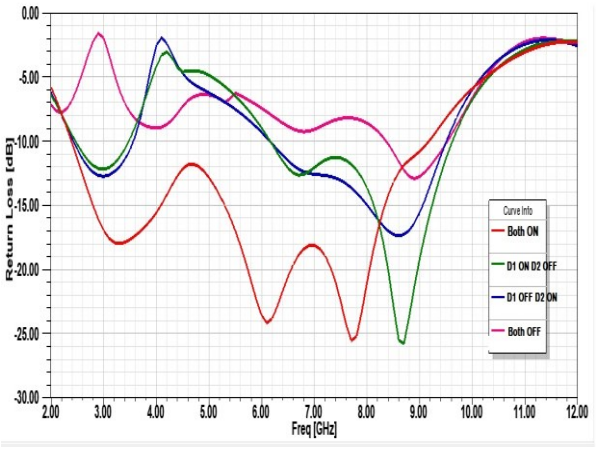

Fig. 3: S11 parameters of a proposed single reconfigurable element

III. PROPOSED FREQUENCY RECONFIGURABLE TWO ELEMENT MIMO ANTENNA

A compact, frequency-reconfigurable MIMO system has been designed using a proposed single element that is operating in various commercial bands Figure 4(a-b) shows the MIMO configuration without and with a stub. The MIMO antenna is realized on a FR4 substrate and has a total volume of 62× 25 ×1.5 mm^3.This MIMO antenna is formed by integrating two single FRA's at proximity of 18mm (0.4λ_0). A common ground plane is shared by the antenna elements, where the separation between ground slots is 16 mm. The antenna elements of MIMO are labelled as Ant1 and Ant2. It is fabricated, and a prototype is produced to authenticate the performance characteristics of modeled MIMO, as shown in Figure 4 (c). A traditional chemical finishing process is used to create the prototype. Key sight Technologies Field Fox Vector Network Analyzer N9926A is used to measure the S-parameters and radiation characteristics.

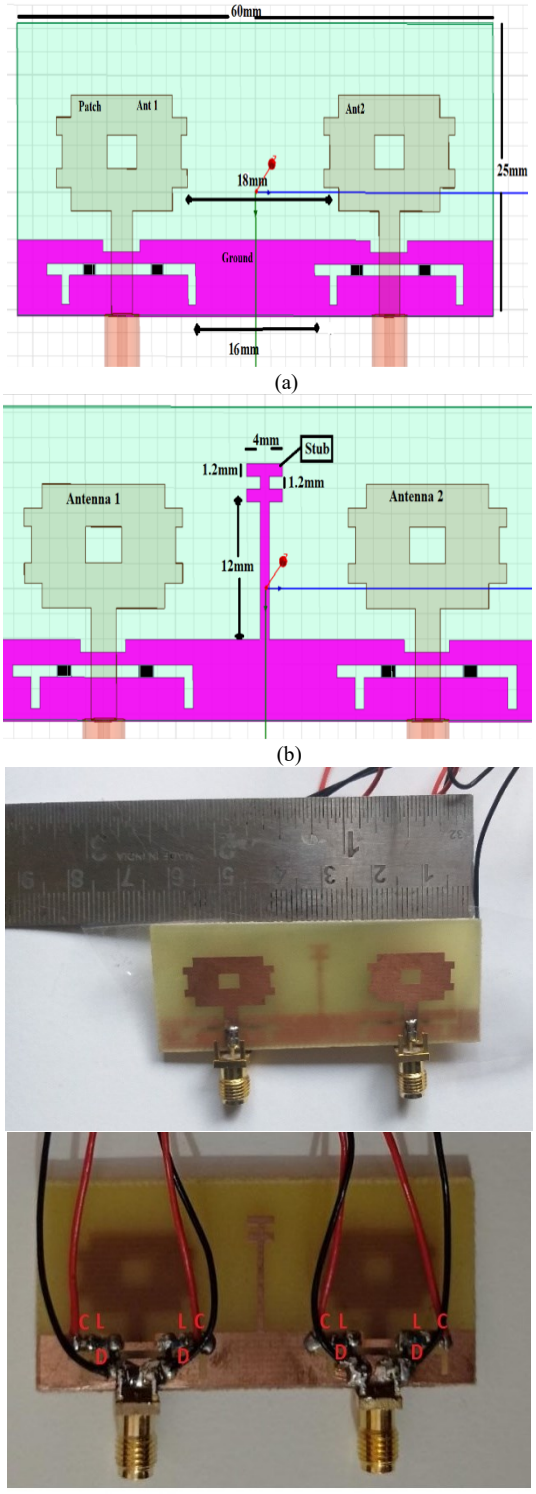

Fig. 4. Proposed MIMO antenna system: (a) proposed layout (b) 2×1 MIMO antenna with stub (c) fabricated circuit top and bottom views

Figure 5 interprets with and without stub reflection coefficients of the simulated MIMO. From figure, observed is integration of stub on the ground plane shifted the passband frequency slightly to the upper side, resulted in a small reduction in bandwidth. This could be due to the stub's resonating property, which is a common issue with this technique and has also been observed in previous research work.

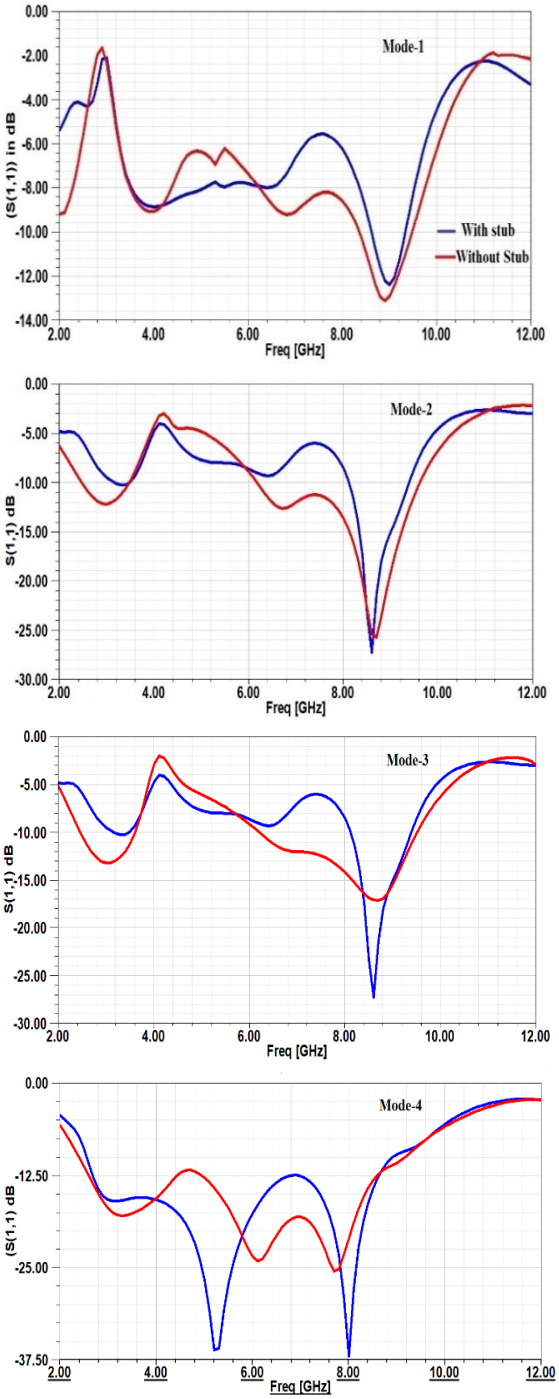

Fig. 5. Comparison of simulated with and without stub S11-parameters

Parallel elements can produce the symmetrical electromagnetic field and the similar polarization thus, the power will flow from antenna 1 to antenna 2 when they are excited, which leads to the high coupling between parallel elements. Figure 6 depicts the simulated surface current distribution when Ant 1 is excited and Ant 2 is terminated at the matched load. The surface waves are linked to the non-excited antenna, causing significant mutual coupling. When stub is incorporated, the surface waves and near fields are blocked from reaching the non-excited antenna by concentrating within the stub, ensuring excellent isolation between the elements.

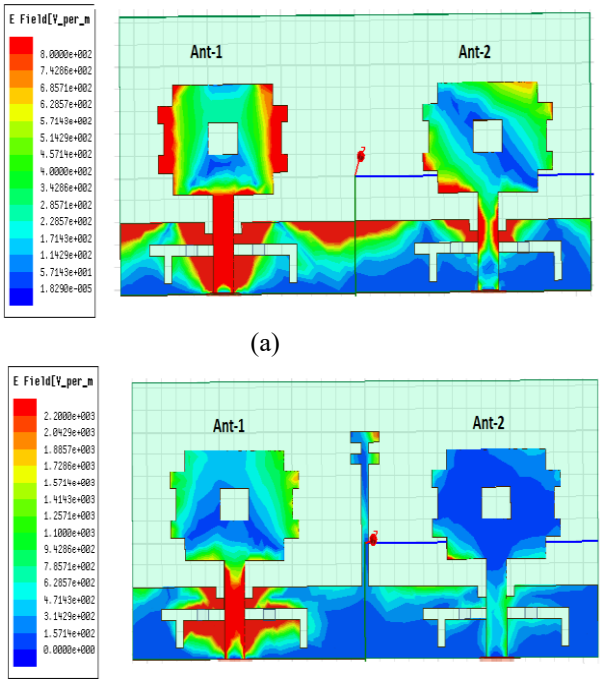

Fig. 6. The simulated surface current distribution(a)without stub and (b)with stub

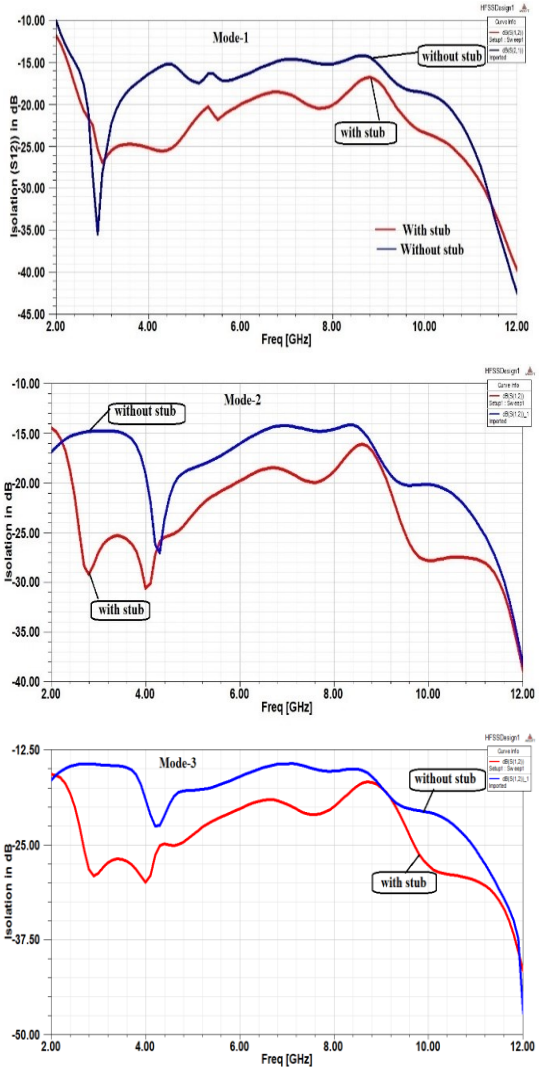

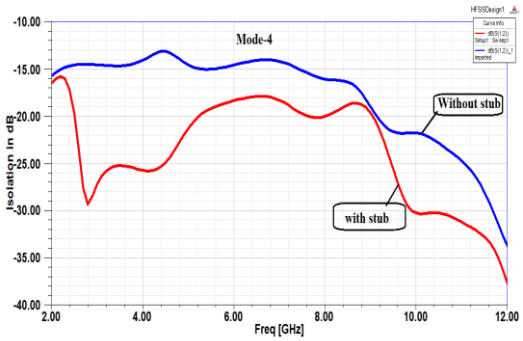

Fig. 7. Comparison of with and without stub S12 of MIMO antenna

Stub significance can also be evaluated by observing the simulated S-parameter and comparing it with those without a stub. Figure 7 compares the isolation of -15 dB achieved without the use of any decoupler at working bands throughout all switching modes. Without stub, isolation values are -14.36, -15, -15.36, -14.89, -15.18, and -14.83 dB at resonance frequencies 8.9, 2.9, 8.7, 3, 8.6, and 5.6 GHz, respectively.

To enhance isolation further, a unique vertical stub is loaded on the ground plane between the radiating elements of the MIMO antenna, as depicted in Figure 4(b). This stub functions as a band-stop filter for the desired band, yielding a transmission null within the radiating elements, which interrupts the flow of current, surface waves, and relative fields. Stub reduces near-field coupling between antenna elements by suppressing surface current transmission and concentrating within the decoupling structure. The dimensions of the stub are shown in Figure 4 (b). The isolation plots in Figure 7 show that the isolation improves significantly upon integrating the stub. In the presence of a stub, the isolation is enhanced to -17.36, -24.70, -17.20, -26.90, -17.20, and -19.62 dB at operating frequencies of f1 = 9 GHz (8.6 to 9.4), f2 = 3.4 GHz (3 to 3.7), f3 = 8.6 GHz (8 to 9.4), f4 = 3.5 GHz (2.8 to 3.8), f5 = 8.5 GHz (7.8 to 9.2), and f6 = 5.4 GHz (2.2 to 9).

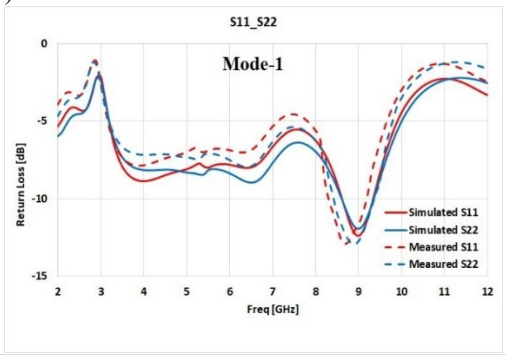

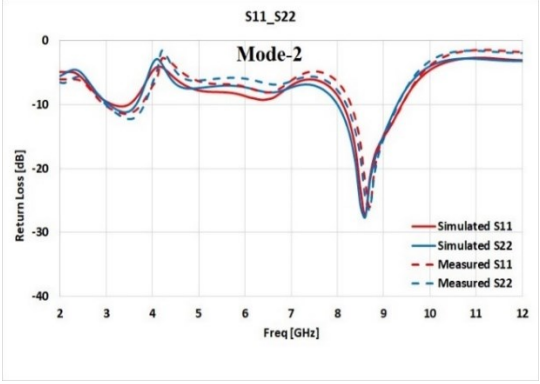

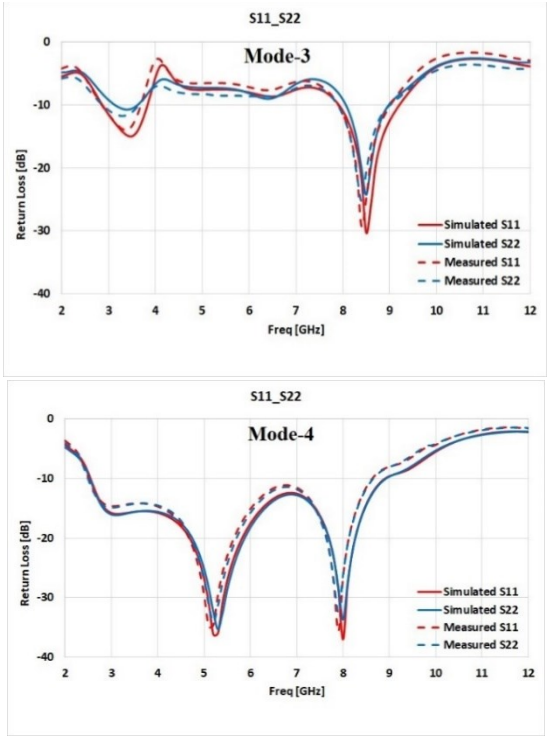

Fig. 8. Comparison between simulated and measured S11-S22 parameters

Figure 8 compares simulated and measured S-parameters. S-parameters(S11) less than –10 dB is measured at frequencies of 8.9 GHz (8.2 to 9.2), 3.5 GHz (3 to 3.9), 8.7 GHz (8.1 to 9.4), 3.4 GHz (2.8 to 3.7), 8.4 GHz (7.7 to 9.1), and 5.4 GHz (2.2 to 9) in four modes. S-parameters indicating that the measured S11 of a stub-based MIMO reconfigurable antenna array replicates the simulated. In addition, measured isolation considerably greater than -18 dB is noticed throughout all functioning bands and switching states, as depicted in Figure 9. In mode 1 at 8.9 GHz, the measured isolation is -18.86. The isolation at 3.5 GHz and 8.7 GHz in state 2 is -27.12 and -18.26 dB, respectively. Isolation at 3.4 and 8.4 GHz in state 3 is -28.40 and -18.76 dB, respectively. The measured isolation at 5.4 GHz is -21.68 in the final state. The simulated and measured isolation parameters are in better agreement. As a result, this paper proposes a simple, compact, and wide band two-element frequency reconfigurable MIMO that can promote diverse wireless applications of 4G technology in LTE band 40 (2.3 GHz to 2.4 GHz), LTE band 42 (3.4 to 3.6 GHz), LTE band 43 (3.6 to 3.8 GHz), LTE band 46 (5.1 to 5.9 GHz), 5G in N77 band (3.2 to 4.2 GHz), sub-6 GHz/N78 band (3.3 to 3.8 GHz), N79 (4.4 to 5GHz), and X band (6.2–9.7 GHz).

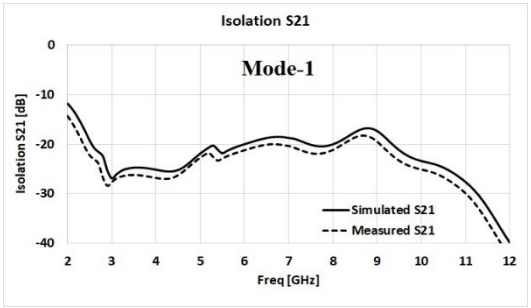

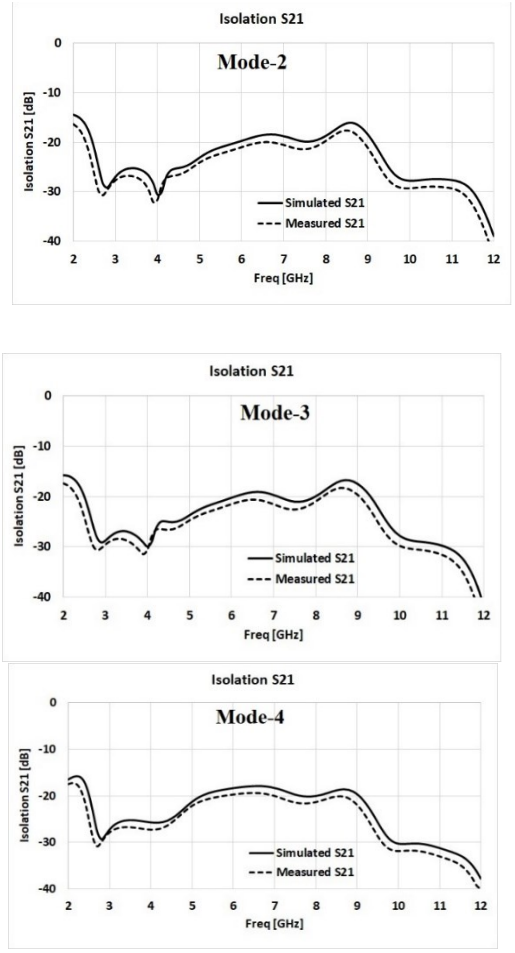

Fig. 9. Comparison between simulated and measured S-parameters (S21)

A. Diversity Performance of MIMO

The radiation patterns of the MIMO antenna were analyzed in an anechoic chamber measuring 8.0 m x 7.0 m x 6.0 m in size. Figure 10 depicts the measured and modelled E- and H-plane patterns atf1= 8.9, f2 = 3.5, f3 = 8.7 GHz, f4 = 3.4, f5=8.4, and f6 = 5.4 GHz. To demonstrate the proposed antenna's performance, the far-field pattern and gain were investigated using an electromagnetic simulator and testing systems. Figure 10 shows an antenna with an omnidirectional radiation pattern in the H-plane and a bidirectional radiation pattern in the E-plane. At 8.9 GHz, the simulated gain is 5.4 dBi, while the measured gain is 5.3 dBi. At 3.5 GHz and 8.7 GHz, the antenna exhibits a nearly omni-directional radiation pattern in the main H-plane (90^0), while the E-plane (0^0) exhibits a bidirectional radiation pattern. The observed simulated gain values are 4.7 dBi and 6.2 dBi, respectively, while the measured values are 4.5 dBi and 6.1 dBi at these frequencies. At 3.4 and 8.4 GHz, the antenna exhibits an omni-directional radiation pattern and a bi-directional radiation pattern in the main H-plane (90^0) and E-plane (0^0), respectively. Furthermore, at 3.4 GHz and 8.4 GHz, a simulated gain of 4.8, 6.3 dBi, is obtained, while a measured gain of 4.5 dBi and 6.2 dBi is obtained. Similarly at 5.4 GHz, the observed simulated gain is 5.6 dBi, while the measured gain is 5.5 dBi.

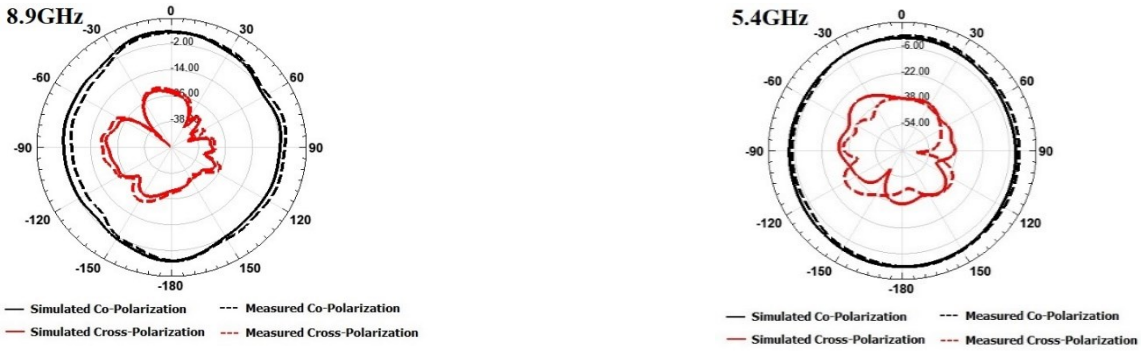

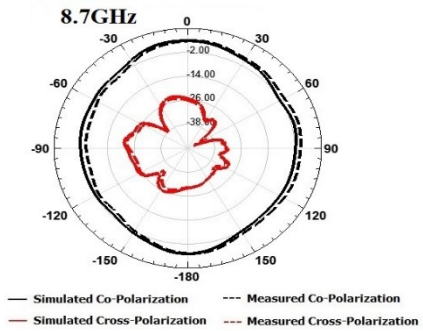

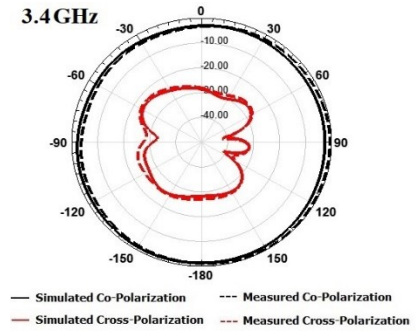

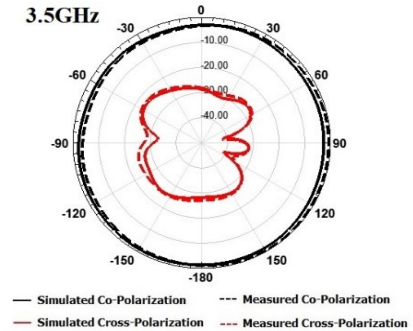

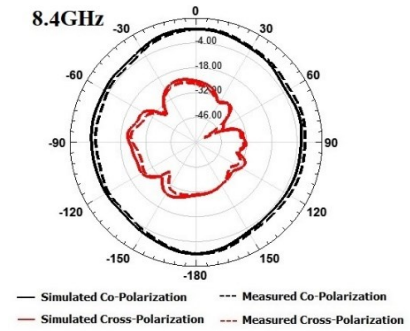

Fig. 10. Comparison between simulated and measured radiation patterns

To evaluate the diversity performance of the MIMO antenna, parameters such as the diversity gain (DG), envelope correlation coefficient (ECC), and channel capacity loss (CCL) were investigated. The ECC result rate the MIMO antenna's multiple-port performance. DG estimates the system's dependability. The CCL, on the other hand, estimates the limit to which information can be transmitted on the channel without loss.

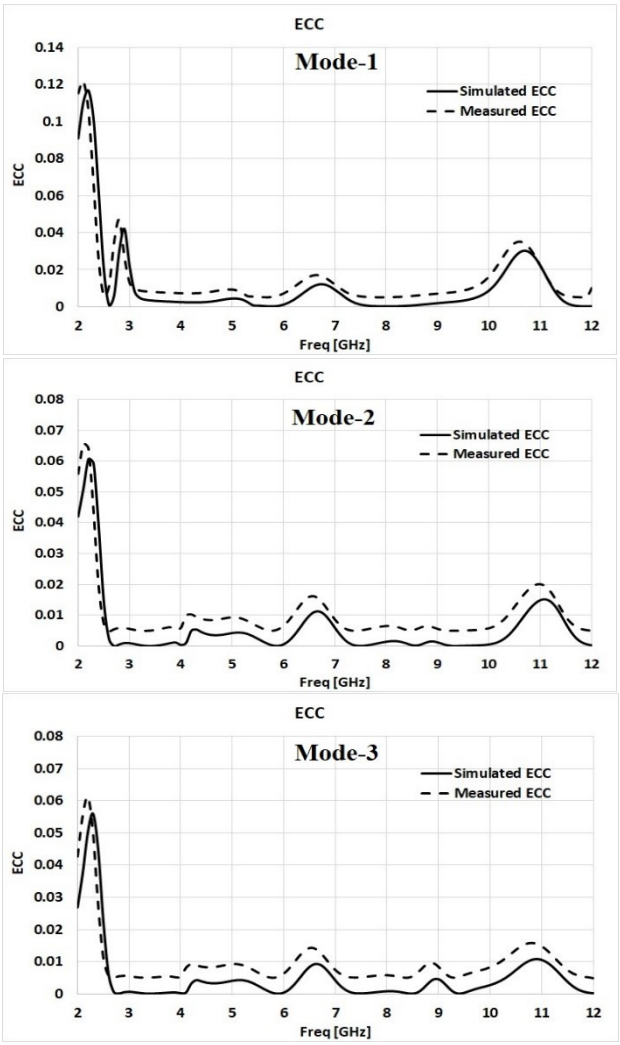

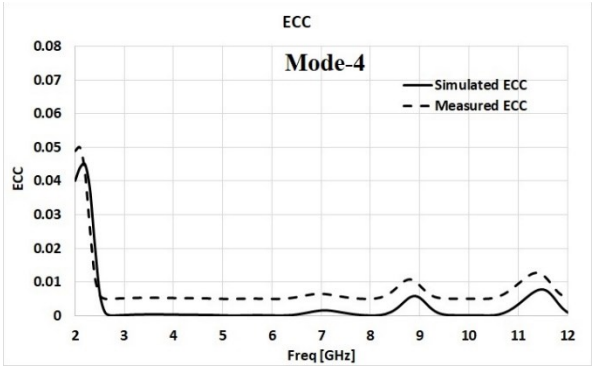

Fig. 11. ECC of the simulated and measured MIMO antenna

Figure 11 illustrates the comparison of the ECC of simulated and measured MIMO antennas. ECC measured is less than 0.0065, which is extremely low when compared to the standard value (0.3) and without a stub value (0.0710). ECC between the elements is calculated using the equation (1) [14], which relies on the measured radiation pattern.

$$\rho_e = \frac{|\int\int \overline{F_1} \cdot \overline{F_2^{\star}} d\Omega|^2}{\int\int |\overline{F_1}|^2 d\Omega \cdot \int\int |\overline{F_2}|^2 d\Omega} \quad (1)$$

where 1 and 2 represent the port numbers. Figure 12 shows the measured and simulated diversity gains in comparison. In all switching states, the stated MIMO antenna simulation and measurement diversity gain values are in close agreement. The DG of all states is > 9.8 dB, implying improved system reliability and diversity performance. The DG is calculated from the ECC using equation (2) [15].

$$DG = 10 \times \sqrt{1 - ECC^2} \quad (2)$$

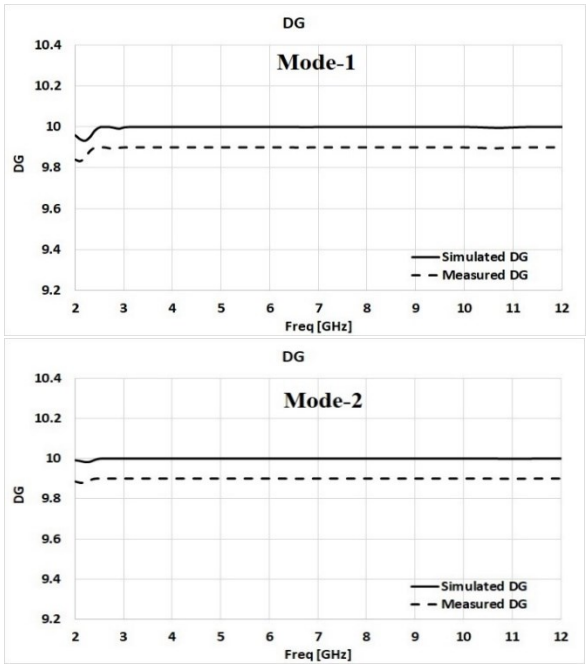

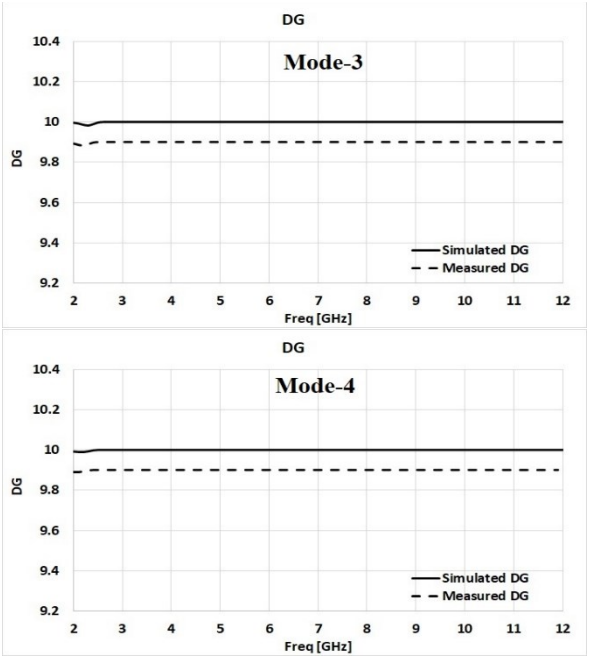

Fig. 12. Comparison of measured and simulated diversity gain

Figure 13 depicts the CCL values of each mode. Simulated and measured CCL values are less than 0.2 b/s/Hz and exhibit quite good CCL performances when compared to the standard value (0.4). Both the ECC and CCL results show that the antenna performs well in terms of diversity.

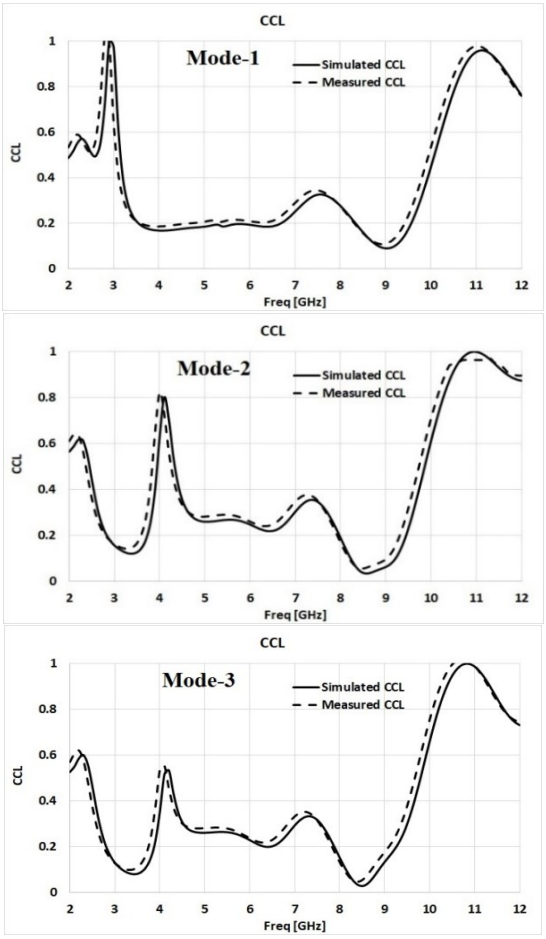

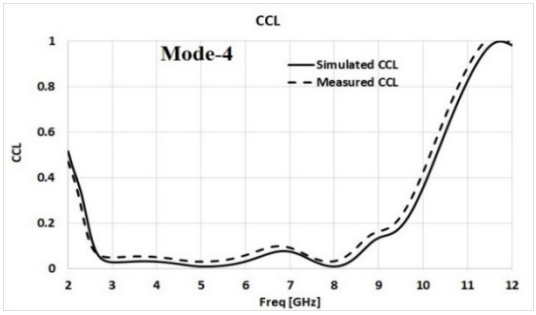

Fig. 13. Simulated and measured with and without stub CCL comparison

Table II illustrates the performance comparison of the recommended and previously published work. The recommended MIMO has less structural complexity, wider frequency coverage, a low profile, and superior results in terms of gain, bandwidth, and better diversity in terms of ECC and CCL. The table demonstrates that suggested antenna has a higher gain than [11, 16–19]. The isolation and ECC however, is comparable to that of [11–19]. There are numerous challenges to designing an FRA-MIMO antenna. The most difficult challenge could be achieving a broad frequency band, higher gain, and adequate isolation between radiating elements. Such a challenge is resolved by the suggested MIMO antenna. Its low profile, wide-bandwidth, higher isolation value and stable omni directional patterns make it suitable for 4G/5G portable devices and others applications.

TABLE II
COMPARES SUGGESTED MIMO WITH EARLIER PUBLISHED WORKS

References	*Dimensions (mm^2)*	*Operating bands*	*Switching device*	*Isolation*	*Gain max.*
[11]	120 × 60	2.2 to 2.7 3.3 to 4.02	RF-PIN Diode	>12dB	4.2
[12]	32 × 98	0.6 – 0.7, 1.7 – 1.9, 2.4 – 2.7, 3.2 – 4.1, 5.1 – 5.9 GHz	RF MEMS	>15dB	5.14
[16]	100x50	1.48, 1.72, 1.9, 2.01, 2.14, 2.27	PIN Diode	>12dB	2.2
[17]	45 × 45	2.2 – 6.28	Non reconfigurable	<−14	3
[18]	60 × 120	0.66 - 1.3, 1.4 - 2.005, 2.42 - 3.09, 3.18 - 3.89	Varactor diode	<11.7	3.9
[19]	150 × 70	3.4–3.6 (−6 dB)	Non reconfigurable	<−12	2.87
Proposed	25×60	8.6 - 9.4 3 - 3.7 8 -9.4 2.8 - 3.6 7.8 – 9.2 2.2 - 9	PIN Diode	>18dB	4.7 to 6.3 dB

CONCLUSION

This paper presents a compact, two-element MIMO antenna that is reconfigurable in frequency to be suitable for 4G/LTE, 5G/sub-6GHz, X-band, INSAT, and ITU band communication. It successfully covers the 8.2 - 9.2GHz, 3 - 3.9GHz, 8.1 - 9.4GHz, 2.8 - 3.7GHz, 7.7 – 9.1GHz and 2.2 – 9GHz bands by electronically switching between four resonance states. Every mode has a reasonable measured peak gain. MIMO provides good diversity performance with a low ECC between the antenna elements and a higher DG (>9.8 dB). Furthermore, the channel capacity loss is less than 0.2bps/Hz, well within the band of each mode. Its compactness and better diversity performance make it ideal for 4G/LTE and 5G portable devices and heterogeneous wireless applications.

REFERENCES

[1] Global update on “Spectrum for 4G and 5G Qualcom technologies”, Available online at https://www.qualcomm.com/media/documents/files/spectrum-for-4g-and-5g.pdf, Jun. 10, 2018.

[2] Abdullah M, Kiani S.H and Iqbal, “Eight element multiple-input multiple-output (MIMO) antenna for 5G mobile applications”, IEEE Acce, vol. 7, pp. 134488-134495, 2019. https://doi.org/10.1109/ACCESS.2019.2941908

[3] Li.A, Luk K.M, Y Li. “A dual linearly polarized end-fire antenna array for the 5G applications”, IEEE Access, 6, 78276–78285, 2018. [CrossRef]

[4] Mudda S, Gayathri K. M and Mudda M, “Compact high gain microstrip patch multi-band antenna for future generation portable devices communication”, International Conference on Emerging Smart Computing and Informatics (ESCI), pp, 471-476, 2021. https://doi.org/10.1109/ESCI50559.2021.9396776

[5] Shivleela Mudda, Gayathri K M, and Mudda Mallikarjun, "Wide-band frequency tunable antenna for 4G, 5G/Sub 6 GHz portable devices and MIMO applications", Progress in Electromagnetics Research C, Vol. 118, 25-41, 2022.

[6] Mudda, S. and Gayathri, K. M," Frequency reconfigurable ultra-wide band MIMO antenna for 4G/5G portable devices applications: review", International Journal on Emerging Technologies,11(3):486–490, 2020.

[7] Alibakhshikenari M, Babaeian F, Virdee B. S, Aissa S, Azpilicueta L, See C. H, AlthuwaybA. A, Huynen I, Abd-Alhameed R. A, Falcone F, & Limiti E, "A comprehensive survey on various decoupling mechanisms with focus on metamaterial and metasurface principles applicable to SAR and MIMO antenna systems", IEEE Access, vol, 8, pp. 192965-193004, 2020. Https://doi.org/10.1109/ACCESS.2020.3032826

[8] Pandit S, Mohan A and Ray P, "Compact Frequency-reconfigurable MIMO antenna for microwave sensing applications in WLAN and WiMAX frequency bands", IEEE Sensors Letters, vol. 2, no. 2, pp. 1-4, Art no. 3500804, 2018. Https://doi.org/10.1109/LSENS.2018.2822598.

[9] Tu D. T. T& Sang N. V., "Frequency reconfigurable multiband MIMO antenna based on gradient arcs for IoT devices", Advanced Electromagnetics, 10(2), 85–93, 2021. https://doi.org/10.7716/aem.v10i2.1524

[10] Hussain, Rifaqat & Khan, Muhammad Umar & Sharawi,Mohammad, "Design and analysis of a miniaturized meandered slot-line-based quad-band frequency agile MIMO antenna", IEEE Transactions on Antennas and Propagation, PP. 1-1. https://doi.org/10.1109/TAP.2019.2943685,2019

[11] Arun Pant, Manish Singh, Manoj Singh Parihar, 2021 "A frequency reconfigurable/switchable MIMO antenna for LTE and early 5G applications", AEU - International Journal of Electronics and Communications, Volume 131, 2021, 153638, ISSN 1434-8411, https://doi.org/10.1016/j.aeue.2021.153638

[12] Muhammad Mateen Hassan, Zeeshan Zahid, Adnan Ahmed Khan, Imran Rashid, Abdul Rauf, Moazam Maqsood & Farooq Ahmed Bhatti, "Two element MIMO antenna with frequency reconfigurable characteristics utilizing RF MEMS for 5G applications", Journal of Electromagnetic Waves and Applications, https://doi.org/10.1080/09205071.2020.1765883.2020

[13] Chithradevi R, Sreeja B, "A compact UWB MIMO antenna with high isolation and low correlation for wireless applications", In Proceedings of the 2017 IEEE International Conference on Antenna Innovations & Modern Technologies for Ground, Aircraft and Satellite Applications (IAIM), Bangalore, *India, 24–26 November 2017*, IEEE: Piscataway, NJ, USA, 2017; pp. 1–4.2017.

[14] Vaughan R. G, Andersen J.B, "Antenna diversity in mobile communications", IEEE Trans, Veh Technol, 36(4):149–172,1987.

[15] Rosengren K, Kildal P.S, "Radiation efficiency, correlation, diversity gain and capacity of a six–monopole antenna array for a MIMO system: theory, simulation and measurement in reverberation chamber", IEEE Proce - Microwaves, Antennas Propag, 152(1):7–16.2005.

[16] Riaz S, Zhao.X, Geng S, "A frequency reconfigurable MIMO antenna with agile feed line for cognitive radio application", International Journal of RF and Microwave Computer-Aided Engineering, 9 pages, Dec. 2019.

[17] Anitha R, Vinesh P. V, Prakash K.C, Mohanan P, Vasudevan K, "A compact quad element slotted ground wideband antenna for MIMO applications", IEEE Trans. Antennas Propag, 64, 4550–4553,2016. [CrossRef].

[18] Hussain R, Khan M. U, and Sharawi M.S, "Design and Analysis of a miniaturized meandered slot-line-based quad-band frequency agile MIMO antenna", IEEE Transactions on Antennas and Propagation, vol. 68, no. 3, pp. 2410-2415. 2020. https://doi.org/10.1109/TAP.2019.2943685

[19] KianiSaad & Altaf, Ahsan & Anjum, Muhammad & Afridi, Sharjeel & Arain, Zulfiqar & Anwar, Sadia & Khan, Salahuddin & Alibakhshikenari, Mohammad & Lalbakhsh, Ali & Khan, Muhammad & Abd-Alhameed, Raed & Limiti, Ernesto, "MIMO antenna system for modern 5G handheld devices with healthcare and high-rate delivery", Sensors, 21. 1-19. https://doi.org/10.3390/s21217415.2021